Nonlinear Dynamics and Systems Theory, **15** (2) (2015) 171–183

Initial Trajectories of Propagation of Fatigue Cracks Under Biaxial Cyclic Loading with Phase Difference

V.Y. Perel * and S. Mall

Air Force Institute of Technology, Department of Aeronautics and Astronautics, 2950 Hobson Way, Wright-Paterson Air Force Base, Ohio 45433-7765, United States

Received: March 4, 2015; Revised: April 2, 2015

Abstract: This paper presents a method for predicting initial trajectories of propagation of two separate fatigue cracks, which are developed under two perpendicular cyclic loads with phase difference between them. Calculation of trajectories of these two initial cracks is the first step in prediction of trajectories and rate of propagation of long cracks. This problem is important for analysis of durability of structures subjected to biaxial loading, where it is necessary to know trajectories of cracks' propagation, stress intensity factors along the trajectories and dependence of cracks' growth rates on stress intensity factors. Existing methods, based on finite element analysis and automatic mesh generation [1,2], allow to perform such calculations only for uniaxial loading and for multi-axial proportional loading, without phase difference between applied external forces. Experiments, presented in this paper, show that under biaxial loading with phase difference between applied loads, two cracks are developed. Comparison of calculated and experimentally observed initial directions of cracks propagation shows that the calculations correctly reflect existence of two cracks and the fact that they are approximately symmetrical about the line that makes 45° with directions of applied loads. This method can become a theoretical basis for extending capabilities of existing methods, based on finite element analysis and automatic mesh generation, of predicting trajectories of fatigue cracks under complex loading conditions.

Keywords: *fatigue; biaxial loading; phase difference; trajectories of cracks propagation.*

Mathematics Subject Classification (2010): 34A34, 34D20, 70E50, 93C15.

* Corresponding author: mailto:victor.perel@yahoo.com

1 Introduction

It has been a common practice to characterize the fatigue crack growth in metals under uniaxial loading. But majority of aerospace structural components experience a combination of axial, bending, shear and torsion stresses, resulting in a complex stress state. It is thus appropriate to extend the fatigue crack growth studies to non-uniaxial loading conditions. For biaxial tension-tension loading without phase difference between applied loads, such studies were performed, for example, by Misak, Perel, Sabelkin and Mall [3]. In the present paper, this study is extended to biaxial tension-tension loading with phase difference between applied loads. Such loading results in growth of two fatigue cracks, as will be shown in this paper. The test material is aluminum alloy 7075-T6, which is widely used as a structural material in the military and civilian aircraft fleet.

Along the direction of crack propagation, the mode II stress intensity factor, K_{II}, is usually much smaller than the mode I stress intensity factor, K_I. So, in the biaxial loading, the dependence of crack growth rate $\frac{da}{dN}$ on the stress intensity factor K_{II} is small, and the dependence of $\frac{da}{dN}$ on K_I can be established experimentally, under uniaxial loading with force normal to the crack. If tips of the crack (or cracks) have different stress intensity factors at any given time instant during the loading cycle, then construction of the cracks' trajectories should be performed with account of relation between $\frac{da}{dN}$ and K_I. This means that if the cracks' trajectories are constructed by an incremental procedure, then, at each step of the procedure, the increments of the cracks' lengths are calculated from the relation between $\frac{da}{dN}$ and K_I, where K_I is a function of crack length, a. But if the tips of the crack have equal stress intensity factors, or if we have one crack originating from an edge, then in constructing the crack's trajectory incrementally, some small straight-line increments of the crack can be specified arbitrarily, without considering $\frac{da}{dN}$. In this case, a number of cycles, N, corresponding to the chosen crack length increment, can be calculated later, in the post-process stage of analysis, using the relation between $\frac{da}{dN}$ and K_I.

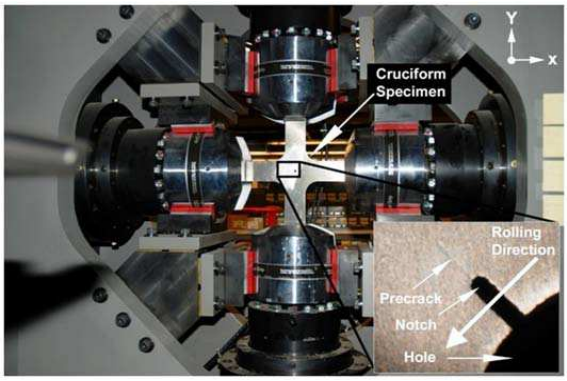

Figure 1a: Experimental setup.

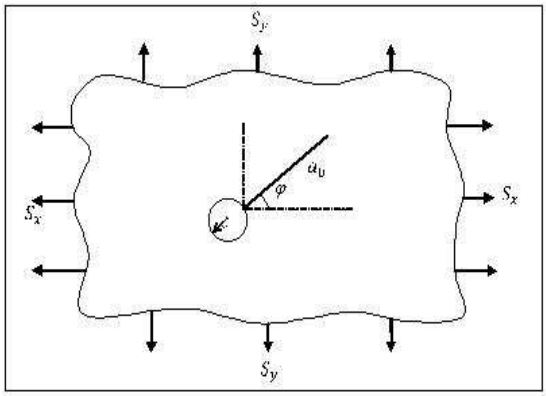

Figure 1b: Pre-crack of length a_0, originating from circular hole of radius r in a thin plate.

2 Direction of Crack Propagation

For construction of the cracks' trajectories, a formula was used for direction of initial crack propagation, based on a hypothesis that crack propagates in the direction $\theta = \Theta$ (Figure 2), in which $\sigma_{\theta\theta}(\theta)$ takes the maximum value (Erdogan and Sih [4]). This hypothesis leads to the formula

$$\Theta = 2 \arctan \frac{1 - \sqrt{1 + 8\left(\frac{K_{II}}{K_I}\right)^2}}{4\frac{K_{II}}{K_I}}. \tag{1}$$

A change of shape of a macroscopic crack in one cycle of loading (or in a small number of cycles) is negligibly small, so at any time instant within one cycle, the angle $\theta = \Theta$ in eq. (1) is measured with respect to a direction of the initial crack (pre-crack), as shown in Figures 1a, 1b and 2.

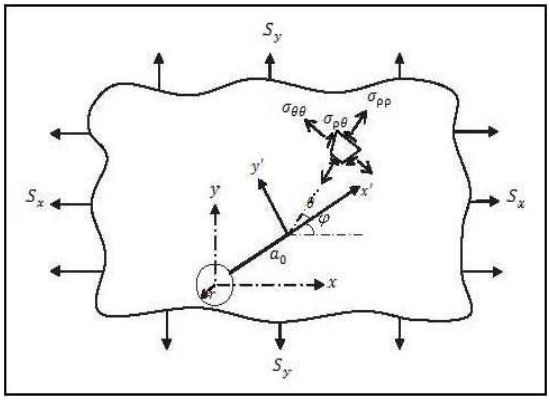

Figure 2: Global rectangular coordinate system xy, local rectangular coordinate system $x'y'$ and polar coordinate system $\rho\theta$.

3 Stress Intensity Factors

In this work, we considered a thin plate of Aluminum 7075-T6, with a pre-crack of length a_0, originating from a circular hole of radius r at angle $\varphi = 45^\circ$ to directions of remote principal stresses S_x and S_y (Figures 1a and 1b). This pre-crack was created by applying sinusoidal loads $S_x(t) = S_y(t)$, without the phase difference between them. After the creation of the pre-crack, the phase difference γ between the loads $S_x(t)$ and $S_y(t)$ was introduced, and the loads became

$$S_x(t) = \frac{(S_x)_{\max} + (S_x)_{\min}}{2} + \frac{(S_x)_{\max} - (S_x)_{\min}}{2} \sin(2\pi\nu t), \tag{2}$$

$$S_y(t) = \frac{(S_y)_{\max} + (S_y)_{\min}}{2} + \frac{(S_y)_{\max} - (S_y)_{\min}}{2} \sin(2\pi\nu t + \gamma). \tag{3}$$

In our experiments and calculations we set

$$\frac{(S_x)_{\min}}{(S_y)_{\min}} = \frac{(S_x)_{\max}}{(S_y)_{\max}} = 1, \qquad \frac{(S_x)_{\min}}{(S_x)_{\max}} = \frac{(S_y)_{\min}}{(S_y)_{\max}} \equiv R = 0.5. \tag{4}$$

For a crack, originating from elliptical hole, at an arbitrary angle to directions of remote principal stresses, a solution for stress intensity factors is given in the paper of Kaminski and Sailov [5]. For the particular case of circular hole and the pre-crack at 45° with the principal stresses, as was the case in our experiments and calculations, this solution takes the form

$$K_I = \frac{\sqrt{\pi r}}{2\sqrt{2}} \sqrt{\frac{l_0 (l_0+2)^3}{(l_0+1)^3}} (S_x + S_y), \tag{5}$$

$$K_{II} = \frac{\sqrt{\pi r}}{2\sqrt{2}} \sqrt{\frac{l_0 (l_0+2)^3}{(l_0+1)^3}} (S_x - S_y), \tag{6}$$

where

$$l_0 = \frac{1}{2} \left(-1 + \frac{a_0}{r} + \sqrt{2\frac{a_0}{r} + \frac{a_0^2}{r^2} + 1} \right). \tag{7}$$

So, for the case of circular hole and the pre-crack at 45° with the principal stresses, we have

$$\frac{K_{II}}{K_I} = \frac{S_x - S_y}{S_x + S_y}. \tag{8}$$

4 Rate of Crack Propagation

4.1 Rate of crack growth due to cyclic variation of load

In considering a small number of loading cycles (several hundred cycles), the change of stress intensity factors is only due to the change of external load with time, since the effect of the change of the crack's shape and length on the stress intensity factors is negligibly small. According to the Dugdale hypothesis, in thin ideally elastic-plastic plates, with a through-thickness crack, plastic strains are concentrated along a narrow layer on the continuation of the crack, so that the plastic zone can be treated as a line of discontinuity of elastic displacement. Therefore, according to the Dugdale hypothesis, a solution for

displacements can be sought as a discontinuous solution based on the elasticity theory. On the basis of this approach, the following formula was obtained by Cherepanov [6] for displacement of one side of the plastic yield strip:

$$v\left(x'\right) = -\frac{2\sigma_Y}{\pi E}\left(2\sqrt{D\left(D-x'\right)} + x' \ln\frac{\sqrt{D}-\sqrt{D-x'}}{\sqrt{D}+\sqrt{D-x'}}\right), \tag{9}$$

where

$$D = \frac{\pi K_I^2}{8\sigma_Y^2} \tag{10}$$

is size of plastic zone in the Dugdale model, σ_Y is yield stress, and E is Young's modulus. During the crack propagation, the strain energy dissipation per unit area of a newly formed surface of the crack (specific energy dissipation) is the path integral along the line of the plastic zone (Cherepanov [6]):

$$\begin{aligned}\gamma_* = \int\limits_{\text{(plastic zone)}} \sigma_{y'y'}\, dv &= \int\limits_0^D \sigma_{y'y'}\left(\frac{\partial v}{\partial x'}dx' + \frac{\partial v}{\partial K_I}\frac{dK_I}{da}dx'\right) \\ &= \sigma_Y \int\limits_0^d \frac{\partial v}{\partial x'}dx' + \sigma_Y \frac{dK_I}{da}\int\limits_0^D \frac{\partial v}{\partial K_I}dx',\end{aligned} \tag{11}$$

where the term $\frac{dK_I}{da}$ is due to increase of length of plastic zone because of change of stress intensity factor (i.e. because of change of load) in a cycle. This term is not related to the growth of the crack.

Substitution of eqs. (9) and (10) into eq. (11) and performing integration gives the result

$$\gamma_* = \frac{K_I^2}{2E} - \frac{\pi}{12E\sigma_Y^2}K_I^3\frac{dK_I}{da}. \tag{12}$$

Introducing notation

$$K_* = \sqrt{2E\gamma_*}, \tag{13}$$

we receive from eq. (12)

$$|da| = \frac{\pi}{6\sigma_Y^2}\left|\frac{K_I^3}{K_*^2 - K_I^2}\, dK_I\right| \tag{14}$$

or

$$\left|\frac{da}{dt}\right| = \frac{\pi}{6\sigma_Y^2}\left|\frac{K_I^3}{K_*^2 - K_I^2}\frac{dK_I}{dt}\right|. \tag{15}$$

It should be noted that here, like in the original work of Cherepanov [6], the formula (15) should be considered as being a semi-empirical one, with K_* treated as a material constant, i.e. the derivations, leading to the formula (15), are not strict, but only such that help to guess this semi-empirical formula. The crack grows $\left(\frac{da}{dt} > 0\right)$ during the crack opening, i.e. when $K_I > 0$ and $\frac{dK_I}{dt} > 0$. Besides, usually, $K_*^2 - K_I^2 > 0$, as will be shown later (Figure 3). Therefore, eq. (15) can be written in a physically meaningful form as

$$\frac{da}{dt} = \frac{\pi}{6\sigma_Y^2}\frac{K_I^3}{K_*^2 - K_I^2}\frac{dK_I}{dt}. \tag{16}$$

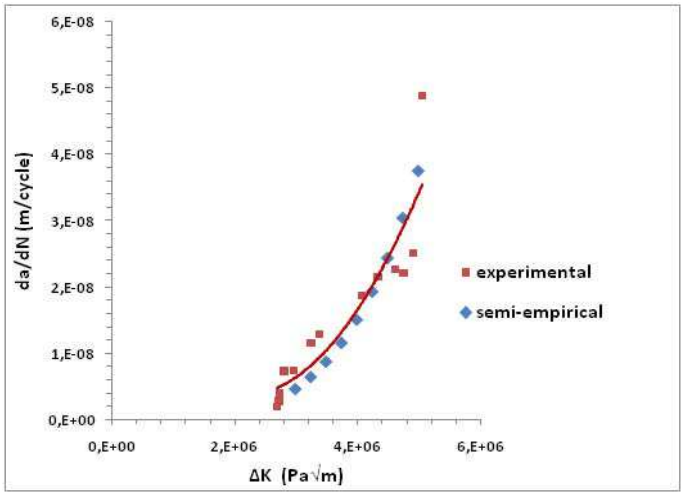

Figure 3: Uniaxial loading, force perpendicular to crack. Comparison of experimental and theoretical curves under the following choice of material constants: $K_* = 4.52459 \times 10^7\ Pa\sqrt{m}$, $\lambda = 4.8353 \times 10^{-7} \frac{1}{Pa\sqrt{m}}$, $\nu_0 = 1.5 \times 10^{-10}\ \frac{m}{s}$.

4.2 Rate of crack growth due to chemical reactions

If the crack grows due to a chemical reaction, for example due to corrosion, then the crack's growth rate $\frac{da}{dt}$ is proportional to the rate of chemical reaction, and, therefore, proportional to $\exp\left(-\frac{U}{RT}\right)$, where U is activation energy of the reaction, T is temperature, and $R = 8.314 \frac{J}{K \times mole}$ is universal gas constant, according to the Arrhenius equation (Arrhenius [7]; Levine [8]). The activation energy U is proportional to stress at the crack tip, and, therefore, to K_I (Cherepanov [6]). Therefore, the crack growth rate due a chemical reaction can be written as

$$\frac{da}{dt} = v_0 \exp\left(\lambda K_I\right), \tag{17}$$

where v_0 and λ are material characteristics that depend on temperature and chemical composition of environment.

4.3 Rate of crack growth due to combined effects of cyclic variation of load and chemical reactions

If the crack grows due to both cyclic variation of K_I and chemical reactions, then the right sides of eqs. (16) and (17) have to be summed up:

$$\frac{da}{dt} = \frac{\pi}{6\sigma_Y} \frac{K_I^3}{K_*^2 - K_I^2} \frac{dK_I}{dt} + v_0 \exp\left(\lambda K_I\right) \tag{18}$$

or

$$a(t) = -\frac{\pi}{12\sigma_Y^2}\left(K_I^2(t) - K_*^2\right) - \frac{\pi K_*^2}{12\sigma_Y^2} \ln\left(K_I^2(t) - K_*^2\right) + v_0 \int \exp(\lambda K_I(t))\, dt + \text{const.} \tag{19}$$

5 Experimental Determination of Material Constants

Eqs. (18) and (19) contain four material characteristics, σ_Y, K_*, v_0 and λ, which need to be determined experimentally. Experimental data on fatigue crack growth rates are usually represented in the form of $\frac{da}{dN}$ versus $\Delta K_I = (K_I)_{\max} - (K_I)_{\min}$, where $(K_I)_{\max}$ and $(K_I)_{\min}$ are maximum and minimum values of K_I in a cycle of loading. So, the theoretical equation (18) or (19) needs to be rewritten in the same form, and then the material characteristics K_*, v_0 and λ in these theoretical equations can be chosen such that the theoretical plot of $\frac{da}{dN}$ versus ΔK_I is close to the experimental one.

As it was mentioned previously, the material characteristics can be established with the use of experimental data obtained in uniaxial loading with remote stress

$$S(t) = \frac{S_{\max} + S_{\min}}{2} + \frac{S_{\max} - S_{\min}}{2} \sin(2\pi\nu t) \tag{20}$$

perpendicular to the crack and the mode I stress intensity factor

$$K_I(t) = \frac{(K_I)_{\max} + (K_I)_{\min}}{2} + \frac{(K_I)_{\max} - (K_I)_{\min}}{2} \sin(2\pi\nu t). \tag{21}$$

Introducing notations

$$R \equiv \frac{S_{\min}}{S_{\max}} = \frac{(K_I)_{\min}}{(K_I)_{\max}}, \quad H \equiv \frac{1+R}{1-R}, \tag{22}$$

we can write eq. (21) as

$$K_I(t) = \frac{1}{2}(\Delta K_I)\left(H + \sin(2\pi\nu t)\right). \tag{23}$$

Crack growth in one cycle of loading occurs during the crack opening, i.e. from the time instant $t = \frac{3}{4\nu}$, when $K_I = (K_I)_{\min} = \frac{R}{1-R}\Delta K_I$, to the time instant $t = \frac{5}{4\nu}$, when $K_I = (K_I)_{\max} = \frac{1}{1-R}\Delta K_I$. Therefore, the increment of the crack length in one cycle of loading, $\frac{da}{dN}$, is

$$\frac{da}{dN} = a\Big|_{K_I = \Delta K_I/(1-R)} - a\Big|_{K_I = \Delta K_I R/(1-R)} = a\Big|_{t=5/(4\nu)} - a\Big|_{t=3/(4\nu)}. \tag{24}$$

Substituting eqs. (19) and (23) into eq. (24), we obtain

$$\begin{aligned} \frac{da}{dN} = &-\frac{\pi K_*^2}{12\sigma_Y^2}\left(H\frac{(\Delta K_I)^2}{K_*^2} + \ln\frac{(1-R)^2 K_*^2 - (\Delta K_I)^2}{(1-R)^2 K_*^2 - R^2(\Delta K_I)^2}\right) \\ &+ v_0 \exp(0.5\lambda H\ \Delta K_I) \int_{\frac{3}{4\nu}}^{\frac{5}{4\nu}} \exp(0.5\lambda\ \Delta K_I\ \sin 2\pi\nu t)\ dt. \end{aligned} \tag{25}$$

In our experiments,

$$\nu = 10Hz, \quad R = 0.5, \quad H = \frac{1+R}{1-R} = 3. \tag{26a}$$

Besides, if our material, Aluminum 7075-T6, is modeled as ideally elastic-plastic, then the yield stress can be taken as

$$\sigma_Y = 4.08249 \times 10^9 Pa. \tag{26b}$$

We need to choose such numerical values of the material constants K_*, v_0 and λ that the graph of $\frac{da}{dN}$ versus ΔK_I, obtained from the semi-empirical formula (25) with numerical values (26), is close to the experimental one. We will try to use the following values

$$v_0 = 1.5 \times 10^{-10} \frac{m}{s}, \quad \lambda = 4.8353 \times 10^{-7} \frac{1}{Pa\sqrt{m}}, \quad K_* = 4.52459 \times 10^7 Pa\sqrt{m}. \tag{27}$$

Substituting numerical values from eqs. (26) and (27) into eq. (25), we receive

$$\begin{aligned} \frac{da}{dN} = & -\left(4.71237 \times 10^{-20}\right) \left(\Delta K_I\right)^2 \\ & - \left(3.21571 \times 10^{-5}\right) \ln \frac{5.11798 \times 10^{14} - \left(\Delta K_I\right)^2}{5.11798 \times 10^{14} - 0.25 \left(\Delta K_I\right)^2} \\ & + \left(1.5 \times 10^{-10}\right) \exp\left(7.25295 \times 10^{-7} \Delta K_I\right) \\ & \times \int_{0.075}^{0.125} \exp\left(2.41765 \times 10^{-7} \Delta K_I \sin 62.8319t\right) dt. \end{aligned} \tag{28}$$

Formula (28) gives the correspondence between numerical values of $\frac{da}{dN}$ and ΔK_I as shown in Table 1.

$\Delta K_I \left(Pa\sqrt{m}\right)$	$\frac{da}{dN}\left(\frac{m}{cycle}\right)$
3×10^6	4.79467×10^{-9}
3.25×10^6	6.60663×10^{-9}
3.5×10^6	8.89594×10^{-9}
3.75×10^6	1.17424×10^{-8}
4×10^6	1.52328×10^{-8}
4.25×10^6	1.94615×10^{-8}
4.5×10^6	2.45306×10^{-8}
4.75×10^6	3.05502×10^{-8}
5×10^6	3.76391×10^{-8}

Table 1:

The plot of data in Table 1, together with experimental plot of $\frac{da}{dN}$ versus ΔK_I for uniaxial loading, is shown in Figure 3. These plots are close to each other. Therefore, numerical values of the material constants v_0, λ and K_* in eq. (27) are chosen correctly.

6 Trajectories of Cracks

Parametric equations of trajectories of cracks, in the local coordinate system $x'y'$ (Figure 2), with axis x' aligned with the pre-crack,

$$x' = x'(t), \quad y' = y'(t) \tag{29}$$

can be written as follows

$$\frac{dx'}{dt} = \frac{da}{dt}\cos\Theta, \quad \frac{dy'}{dt} = \frac{da}{dt}\sin\Theta. \tag{30}$$

Experiments show that under biaxial tensile and compressive loading with phase difference between applied loads (Figures 1a and 1b), two cracks originate from the pre-crack, and their trajectories are approximately symmetrical about the line along the pre-crack (Figures 4b, 5b, 6b). Therefore, it is assumed that in the first half-cycle of loading, one of the cracks grows starting from the edge of the pre-crack; and in the second half-cycle of loading, the second crack grows starting from the same location, i.e. from the edge of the pre-crack. So**,** initial conditions for the first half-period of loading are

$$x'(0) = 0, \quad y'(0) = 0, \tag{31}$$

and initial conditions for the second half-period are

$$x'\left(\frac{T}{2}\right) = 0, \quad y'\left(\frac{T}{2}\right) = 0, \tag{32}$$

where T is the time duration of one cycle of loading. A solution of differential equations (30) for the first half-period of loading (for crack branch 1), i.e. a solution with initial conditions (31), is

$$x'(t) = \int_0^t \frac{da}{dt}\cos\Theta, \quad y'(t) = \int_0^t \frac{da}{dt}\sin\Theta\, dt. \tag{33}$$

A solution of differential equations (30) for the second half-period of loading (for crack branch 2), i.e. a solution with initial conditions (32), is

$$x'(t) = \int_{T/2}^t \frac{da}{dt}\cos\Theta\, dt, \quad y'(t) = \int_{T/2}^t \frac{da}{dt}\sin\Theta\, dt. \tag{34}$$

If a small number of cycles is considered, during which the effect of change of cracks' shapes and lengths on values of the stress intensity factors is negligibly small (several hundred cycles), then a complete system of equations, leading to calculation of the cracks' trajectories, is

$$S_x(t) = \frac{(S_x)_{\max} + (S_x)_{\min}}{2} + \frac{(S_x)_{\max} - (S_x)_{\min}}{2}\sin(2\pi\nu t), \qquad \text{eq. (2)}$$

$$S_y(t) = \frac{(S_y)_{\max} + (S_y)_{\min}}{2} + \frac{(S_y)_{\max} - (S_y)_{\min}}{2}\sin(2\pi\nu t + \gamma), \qquad \text{eq. (3)}$$

$$\frac{K_{II}}{K_I} = \frac{S_x - S_y}{S_x + S_y}, \qquad \text{eq. (8)}$$

$$\Theta = 2\arctan\frac{1 - \sqrt{1 + 8\left(\frac{K_{II}}{K_I}\right)^2}}{4\frac{K_{II}}{K_I}}, \qquad \text{eq. (1)}$$

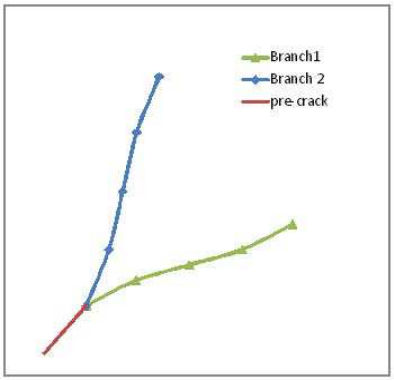

Figure 4a: Calculated trajectories of propagation of cracks in the first cycle of loading, when phase difference between applied loads was 180°.

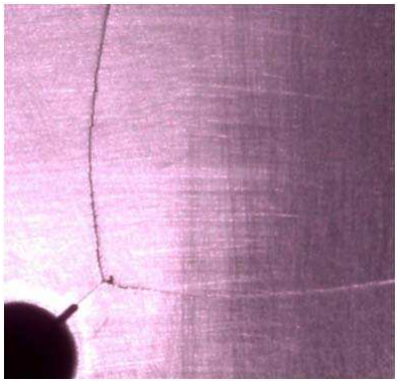

Figure 4b: Trajectories of propagation of cracks, observed in experiment, when phase difference between applied loads was 180°.

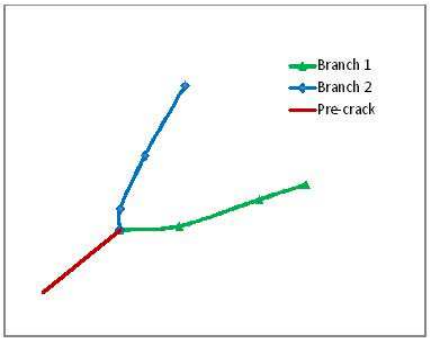

Figure 5a: Calculated trajectories of propagation of cracks in the first cycle of loading, when phase difference between applied loads was 90°.

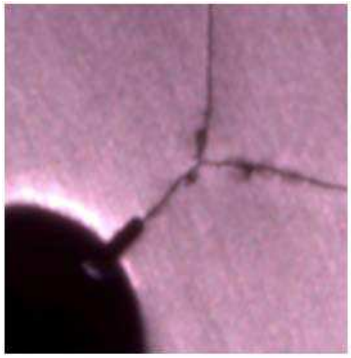

Figure 5b: Trajectories of propagation of cracks, observed in experiment, when phase difference between applied loads was 90°.

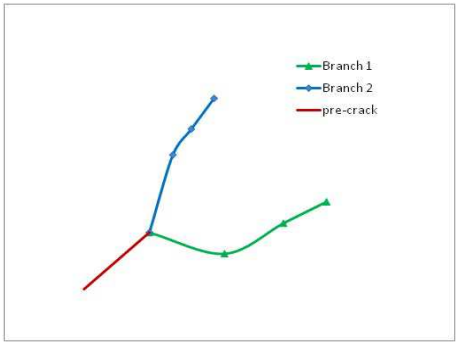

Figure 6a: Calculated trajectories of propagation of cracks in the first cycle of loading, when phase difference between applied loads was 45°.

$$l_0 = \frac{1}{2}\left(-1 + \frac{a_0}{r} + \sqrt{2\frac{a_0}{r} + \frac{a_0^2}{r^2} + 1}\right), \qquad \text{eq. (7)}$$

$$K_I = \frac{\sqrt{\pi r}}{2\sqrt{2}}\sqrt{\frac{l_0(l_0+2)^3}{(l_0+1)^3}}(S_x + S_y), \qquad \text{eq. (5)}$$

$$\frac{da}{dt} = \frac{\pi}{6\sigma_Y^2}\frac{K_I^3}{K_{Ic}^2 - K_I^2}\frac{dK_I}{dt} + v_0 \exp\left(\lambda K_I\right), \qquad \text{eq. (18)}$$

$$x'(t) = \int_0^t \frac{da}{dt}\cos\Theta\, dt, \quad y'(t) = \int_0^t \frac{da}{dt}\sin\Theta\, dt \quad \text{for branch 1,} \qquad \text{eq. (33)}$$

$$x'(t) = \int_{T/2}^t \frac{da}{dt}\cos\Theta\, dt, \quad y'(t) = \int_{T/2}^t \frac{da}{dt}\sin\Theta\, dt \quad \text{for branch 2.} \qquad \text{eq. (34)}$$

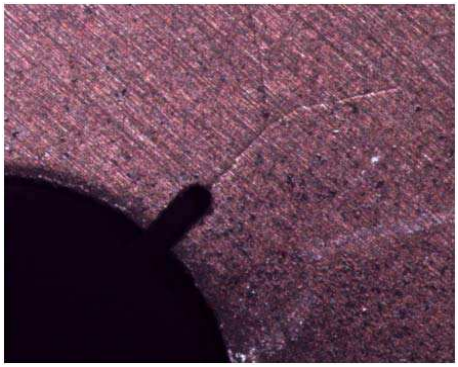

Figure 6b: Trajectories of propagation of cracks, observed in experiment, when phase difference between applied loads was 45°.

Coordinates of points of the cracks' trajectories in the global coordinate system xy can be calculated by formulas

$$\begin{aligned} x &= x' \cos\varphi - y' \sin\varphi, \\ y &= x' \sin\varphi + y' \cos\varphi, \end{aligned} \tag{35}$$

where φ is angle between axes x' and x, i.e. angle between the pre-crack and the axis x (Figure 2).

Alternatively, the cracks' trajectories can be calculated by incremental procedure, which can be written briefly as follows:

$$t_0 = 0, \quad t_m = \frac{m}{M}\frac{T}{2}, \tag{36a}$$

$$m = 1, 2, \ldots, M \quad \text{for first half-cycle,} \tag{36b}$$

$$m = M+1, \ldots, 2M \quad \text{for second half-cycle,} \tag{36c}$$

where $2M$ is a number of equal sub-intervals into which time interval of one cycle of loading, $[0, T]$, is divided;

$$x'_m = x'(t_m), \quad y'_m = y'(t_m), \quad \Theta_m = \Theta(t_m), \quad a_m = a(t_m), \quad \Delta a_m = a_m - a_{m-1}, \tag{37}$$

$$x'_0 = 0, \quad y'_0 = 0, \quad \Theta_0 = 0, \tag{38}$$

$$x'_m = x'_{m-1} + (\Delta a_m)\cos\Theta_m, \tag{39}$$

$$y'_m = y'_{m-1} + (\Delta a_m)\sin\Theta_m. \tag{40}$$

The calculated trajectories of cracks' propagation in the first cycle of loading, with phase differences 180°, 90° and 45°, are shown in Figures 4a, 5a and 6a accordingly. The corresponding experimentally observed initial directions of cracks' propagation are shown in Figures 4b, 5b and 6b accordingly. Comparison of the calculated and experimentally observed initial directions shows that the calculations correctly reflect existence of two initial cracks and the fact that they are approximately symmetrical about the line along the pre-crack.

7 Conclusion

It should be noted again that calculations of cracks' trajectories, presented in this paper, can be valid only for a small number of cycles (several hundred cycles), during which the stress intensity factors are not significantly affected by change of cracks' shapes and lengths. Therefore, calculations in this paper can be used for prediction of cracks' trajectories only during a small initial number of cycles. But if the cracks' trajectories need to be calculated for a larger number of cycles, then values of stress intensity factors should be recalculated after every several thousand cycles with the use of the finite element method, to take account of effect of change of the cracks' shapes and lengths on the stress intensity factors. Besides, in calculations of the cracks' trajectories over intervals of large number of cycles, the angle Θ, given by eq. (1), should be treated as an angle between the current direction of the crack propagation and the direction before the latest block of several thousand cycles was applied. In other words, for long cracks, Θ should be treated not as an angle between a direction of the tangent to the crack at its tip and the direction of the straight-line pre-crack (as it was done in this paper), but as an increment of this angle in the current sub-interval of loading. Such calculations of trajectories of long cracks under biaxial loading with phase difference can be a subject of future work.

Acknowledgement

The authors gratefully acknowledge the support of Office of Corrosion Policy and Oversight, OSD, Washington, DC (Mr. Richard A. Hays).

References

[1] Carter, B.J., Wawrzynek, P.A. and Ingraffea, A.R. Automated 3-D crack growth simulation. *Int. J. Num. Meth. Eng.* **47** (2000) 229–253.

[2] FRANC3D, Abaqus Tutorial, Version 6. http://www.fracanalysis.com/Franc3D_Documentation. Accessed 25 February 2015.

[3] Misak, H.E., Perel, V.Y., Sabelkin, V. and Mall, S. Crack growth behavior of 7075-T6 under biaxial tension-tension fatigue. *Int. J. Fatigue* **55** (2013) 158–165.

[4] Erdogan, F. and Sih, G.C. On the crack extension in plates under plane loading and transverse shear. *Trans. ASME J. Basic. Eng.* **85** (4) (1963) 519–527.

[5] Kaminski, A.A. and Sailov, N.S. Spreading of cracks from the contours of elliptical openings in brittle plates under biaxial tensile stresses. *Soviet Applied Mechanics* **11** (2) (1975) 167–173.

[6] Cherepanov, G. P. *Mechanics of Brittle Fracture.* McGraw-Hill, 1979.

[7] Arrhenius, S.A. Über die Reaktionsgeschwindigkeitbei der Inversion von Rohrzucker durch Säuren. *Z. Physik Chem.* **4** (1889) 226–248. [German]

[8] Levine, R.D. *Molecular Reaction Dynamics.* Cambridge University Press, 2005.